

First-principles study of electronic and magnetic properties of self-intercalated van der Waals magnet $Cr_3Ge_2Te_6$

Jia-wan Li(李家万), Shi-Bo Zhao(赵世博), Lin Zhuang(庄琳), and Yusheng Hou(侯玉升)

Citation: Chin. Phys. B, 2025, 34 (**3**): 036301. DOI: 10.1088/1674-1056/adab67
Journal homepage: http://cpb.iphy.ac.cn; http://iopscience.iop.org/cpb

What follows is a list of articles you may be interested in

Stable structures and properties of Ru_2Al_5

Jing Luo(罗晶), Meiguang Zhang(张美光), Xiaofei Jia(贾晓菲), and Qun Wei(魏群)
Chin. Phys. B, 2025, 34 (**1**): 016301. DOI: 10.1088/1674-1056/ad92fe

Strain-tuned electronic and valley-related properties in Janus monolayers of $SWSiX_2$ (X = N, P, As)

Yunxi Qi(戚云西), Jun Zhao(赵俊), and Hui Zeng(曾晖)
Chin. Phys. B, 2024, 33 (**9**): 096302. DOI: 10.1088/1674-1056/ad6077

Two-dimensional $Cr_2Cl_3S_3$ Janus magnetic semiconductor with large magnetic exchange interaction and high-T_c

Lei Fu(伏磊), Shasha Li(李沙沙), Xiangyan Bo(薄祥奘), Sai Ma(马赛), Feng Li(李峰), and Yong Pu(普勇)
Chin. Phys. B, 2024, 33 (**9**): 096301. DOI: 10.1088/1674-1056/ad5538

First-principles study on stability and superconductivity of ternary hydride $LaYH_x$ (x =2, 3, 6 and 8)

Xiao-Zhen Yan(颜小珍), Xing-Zi Zhou(周幸姿), Chao-Fei Liu(刘超飞), Yin-Li Xu(徐寅力), Yi-Bin Huang(黄毅斌), Xiao-Wei Sheng(盛晓伟), and Yang-Mei Chen(陈杨梅)
Chin. Phys. B, 2024, 33 (**8**): 086301. DOI: 10.1088/1674-1056/ad41b8

Structure and dynamical properties during solidification of liquid aluminum induced by cooling and compression

Min Wu(吴旻), Yong-Qi Yang(杨永琪), and Yao Wang(王垚)
Chin. Phys. B, 2024, 33 (**7**): 076301. DOI: 10.1088/1674-1056/ad39d0

First-principles study of electronic and magnetic properties of self-intercalated van der Waals magnet $Cr_3Ge_2Te_6$

Jia-wan Li(李家万), Shi-Bo Zhao(赵世博), Lin Zhuang(庄琳), and Yusheng Hou(侯玉升)†

Guangdong Provincial Key Laboratory of Magnetoelectric Physics and Devices, Center for Neutron Science and Technology, School of Physics, Sun Yat-Sen, Guangzhou 510275, *China*

(Received 27 November 2024; revised manuscript received 8 January 2025; accepted manuscript online 17 January 2025)

Self-intercalated van der Waals magnets, characterized by self-intercalating native atoms into van der Waals layered structures with intrinsic magnetism, exhibit a variety of novel physical properties. Here, using first-principles calculations and Monte Carlo simulations, we report a self-intercalated van der Waals ferromagnet, $Cr_3Ge_2Te_6$, which has a high Curie temperature of 492 K. We find that $Cr_3Ge_2Te_6$ is nearly half-metallic with a spin polarization reaching up to 90.9%. Due to the ferromagnetism and strong spin–orbit coupling effect in $Cr_3Ge_2Te_6$, a large anomalous Hall conductivity of 138 $\Omega^{-1}\cdot cm^{-1}$ and 305 $\Omega^{-1}\cdot cm^{-1}$ can be realized when its magnetization is along its magnetic easy axis and hard axis, respectively. By doping electrons (holes) into $Cr_3Ge_2Te_6$, these anomalous Hall conductivities can be increased up to 318 $\Omega^{-1}\cdot cm^{-1}$ (648 $\Omega^{-1}\cdot cm^{-1}$). Interestingly, a five-layer $Cr_3Ge_2Te_6$ thin film retains room-temperature ferromagnetism with a higher spin polarization and larger anomalous Hall conductivity. Our study demonstrates that $Cr_3Ge_2Te_6$ is a novel room-temperature self-intercalated ferromagnet with high-spin polarization and large anomalous Hall conductivity, offering great opportunities for designing nano-scale electronic devices.

Keywords: self-intercalated van der Waals magnet, room-temperature ferromagnet, near half-metallicity, large anomalous Hall conductivity

PACS: 63.20.dk, 71.15.Mb, 75.50.Cc, 71.20.–b

DOI: 10.1088/1674-1056/adab67 **CSTR:** 32038.14.CPB.adab67

1. Introduction

Since atomically thin graphene was mechanically exfoliated from conventional van der Waals (vdW) layered graphite in 2004,[1] the research into vdW layered materials has triggered significant interest.[2] In particular, magnetic vdW materials featuring intrinsic magnetism provide an additional degree of freedom, i.e., the spin of the electron, which potentially offers greater opportunities for manipulating electronic states.[3,4] For instance, recent studies have observed intriguing phenomena such as the giant magneto-optical effect in vdW room-temperature ferromagnet Fe_3GaTe_2 and large room-temperature magnetoresistance in its heterostructures.[5,6] Furthermore, the coexistence of cleavable properties and magnetism makes vdW magnets an ideal platform for exploring magnetism in the two-dimensional (2D) limit.[7] Experimental discoveries of FM order in the 2D thin film of Cr-based vdW magnets CrI_3[8] and $Cr_2Ge_2Te_6$[9] underscore their potential. However, despite extensive research, the low magnetic critical temperature (T_C) in these 2D vdW magnets hinders their practical applications in spintronic devices.

By intercalating foreign guest species, e.g., lithium and tetrabutyl ammonium, into the vdW gap of these layered magnets, their T_Cs can be greatly enhanced and their practical applications in spintronic devices is thereby enabled.[10,11] However, the ill-defined intercalated phase in these intercalated vdW magnets renders their theoretical study difficult. Intercalating native atoms into transition metal dichalcogenides (TMDs), a new class of self-intercalated vdW magnets with the advantages of high-quality products, well-defined phases and long-range crystalline order have received more and more attention.[12] Among them, a series of non-ferromagnetic (Ti-, Co-, Nb-, Mo-, Ta-based) TMDs develop FM order upon self-intercalation.[13] In the case of those with intrinsic magnetism, such as FM $CrTe_2$, different stoichiometric self-intercalated $Cr_{1+\delta}Te_2$ ($0 < \delta < 1$) phases are produced by intercalating Cr atoms under growth. These novel phases can retain the ferromagnetism and induce novel magnetic and topological properties.[14] For example, strong magnetic anisotropy and colossal anomalous Hall effect (AHE) have been observed in Cr_5Te_8.[15–17] A giant topological Hall effect has been noted in room-temperature ferromagnet $Cr_{0.82}Te$.[18] In addition, a topological Hall effect, along with potential magnetic skyrmion phase, has been identified in Cr_2Te_2.[19] A Néel-type skyrmion phase below 200 K has been observed in acentric self-intercalated Cr_2Te_3.[20] Thickness-dependent magnetic biskyrmions have been found in Cr_3Te_4 nanosheet.[21] Lastly, room-temperature magnetic skyrmions have been reported in self-intercalated $Cr_{1.53}Te_2$.[22]

Recently, another self-intercalated vdW magnet with a ferrimagnetic (FiM) order, $Mn_3Si_2Te_6$, has also drawn in-

†Corresponding author. E-mail: houysh@mail.sysu.edu.cn

© 2025 Chinese Physical Society and IOP Publishing Ltd. All rights, including for text and data mining, AI training, and similar technologies, are reserved.

tensive research interest for its colossal magnetoresistance (MR).[23–33] One of the most inspiring characteristics is its spin orientation-dependent MR, which changes by seven orders of magnitude when a magnetic field is applied along its magnetic hard axis.[23,24] When $Mn_3Si_2Te_6$ is thinned down to 2D limit, its nanoflakes can exhibit an electrically gate-tunable MR with a faster response.[31] In addition, an unconventional chiral orbital current state flowing along the edges of $MnTe_6$ octahedra enables the current-sensitive giant Hall effect in $Mn_3Si_2Te_6$.[26,34] Theoretically, switchable in-plane AHE by magnetization orientation is put forward in $Mn_3Si_2Te_6$ monolayer.[35] Other merits in $Mn_3Si_2Te_6$, such as magnetocaloric effect,[36] low thermal conductivity[37,38] and anomalous Nernst effect,[39] imply its potential applications in thermoelectricity. The enhanced ultrafast terahertz conductivity[40] and large magneto-optical effects[41] highlight the photoelectric applications of $Mn_3Si_2Te_6$. Considering that the low T_C ($\sim$ 78 K) of $Mn_3Si_2Te_6$[42] hinders its practical applications of these abundant exotic properties, some strategies, including high pressure[27,29,32,33] and electron doping,[43] are proposed to boost its T_C. However, the T_C of $Mn_3Si_2Te_6$ in these studies is still lower than room temperature, highlighting the need to find new self-intercalated vdW magnets.

In this paper, we systematically investigate the electronic and magnetic properties of a novel self-intercalated vdW magnet $Cr_3Ge_2Te_6$, a sibling of $Mn_3Si_2Te_6$, using first-principles calculations and Monte Carlo simulations. Unlike $Mn_3Si_2Te_6$, which is FiM and has a low T_C, our DFT calculations reveal that $Cr_3Ge_2Te_6$ is thermodynamically stable and an in-plane ferromagnet with a high T_C of 492 K, which is a prerequisite for practical applications. By examining its band structures, we find that $Cr_3Ge_2Te_6$ is nearly half-metallic with a spin polarization of 90.9%. As a result of the ferromagnetism and the strong spin–orbit coupling (SOC) effect, $Cr_3Ge_2Te_6$ exhibits an anomalous Hall conductivity (AHC) of 138 $\Omega^{-1}\cdot\mathrm{cm}^{-1}$. When its magnetization is regulated along the hard axis (i.e., the z axis), $Cr_3Ge_2Te_6$ has a larger AHC of 305 $\Omega^{-1}\cdot\mathrm{cm}^{-1}$. Because the AHC is sensitive to the Fermi level, it can be further enhanced by doping electrons or holes into $Cr_3Ge_2Te_6$. Lastly, we show that a five-layer (5L) $Cr_3Ge_2Te_6$ thin film also possesses in-plane ferromagnetism with a high T_C above room temperature and a higher spin polarization of 99.8%. When the 5L $Cr_3Ge_2Te_6$ thin film has an out-of-plane magnetization, its AHC can be as large as 350 $\Omega^{-1}\cdot\mathrm{cm}^{-1}$ and can further increase up to 731 $\Omega^{-1}\cdot\mathrm{cm}^{-1}$ through doping holes. It is worth noting that the high T_C, high-spin polarization and out-of-plane AHE in the 5L $Cr_3Ge_2Te_6$ thin film is different from the magnetic properties and in-plane AHE in the $Mn_3Si_2Te_6$ thin film.[31,35] Our study demonstrates that the room-temperature ferromagnetism, high-spin polarization and large AHC in the vdW self-intercalated magnet $Cr_3Ge_2Te_6$ may provide opportunities for developing intriguing spintronic devices.

2. Computational methods

Our first-principles calculations based on the density functional theory (DFT) are performed using the Vienna *ab initio* simulation package (VASP)[44] at the level of the generalized gradient approximation with Perdew–Burke–Ernzerhof potential.[45] The pseudopotentials with valence electrons of Cr $3d^54s^1$, Ge $4s^24p^2$ and Te $5s^25p^4$ are utilized through the projector augmented wave method.[46,47] The cutoff energy is 350 eV and the total energy criterion at the self-consistent step is set to be 10^{-6} eV. In structural relaxations, the lattice constants and atomic positions are fully relaxed until the force acting on each atom is smaller than 0.01 eV/Å. Furthermore, the local-spin-density approximations plus U (LSDA+U) method[48] and the effective Coulomb interaction $U_{\mathrm{eff}} = 2.0$ eV with $U = 3.0$ eV and $J_{\mathrm{H}} = 1.0$ eV are adopted to describe the strong correlation effects among 3d electrons of Cr.[49] Based on the magnetic parameters obtained from DFT calculations, we perform Monte Carlo simulations using the Metropolis algorithm to explore magnetic ground states and T_C. The 5L $Cr_3Ge_2Te_6$ thin film is built with a vacuum space of 15 Å to avoid spurious interactions.

3. Results and discussion

Figure 1(a) shows the self-intercalated vdW structure of $Cr_3Ge_2Te_6$, which consists of two different Cr sites (denoted as Cr1 and Cr2, respectively). The layers formed by Cr1 atoms, where $CrTe_6$ octahedra share edges within the *ab* plane, are analogous to the honeycomb structure of $Cr_2Ge_2Te_6$. Cr2 atoms are intercalated between two Cr1 layers, and their half-filled structures in the vdW gap form a Cr2-trigonal layer. Thus, as shown in Fig. 1(b), Cr1-honeycomb and Cr2-trigonal layers alternately stack along the c axis, giving rise to the same trigonal space group $P\bar{3}1c$ as $Mn_3Si_2Te_6$.[42] Our calculations show that the lattice constants of $Cr_3Ge_2Te_6$ are $a = b = 7.12$ Å and $c = 14.52$ Å, which are comparable to those in $Mn_3Si_2Te_6$ ($a = b = 7.03$ Å, $c = 14.25$ Å). This is understandable because the Cr atom with a $3d^54s^1$ electronic configuration has a similar radius to Mn ($3d^54s^2$).[42] In $Cr_3Ge_2Te_6$, the Ge–Ge bond length along the c axis is 2.47 Å, comparable with that in $Cr_2Ge_2Te_6$.[50] This indicates that Ge atoms form Ge–Ge dimers. As a result, Ge atoms have a valence state of 3+. In addition, Te atoms commonly exhibit a valence state of 2− due to their strong electronegativity. Consequently, Cr atoms are in a formal 2+ valence state and have a $3d^4$ configuration to maintain the electrical neutrality in $Cr_3Ge_2Te_6$. Our calculated magnetic moments for Cr1 and Cr2 atoms are 3.86 μ_B/Cr and 4.06 μ_B/Cr, respectively. These indicate that Cr^{2+} cations have a high-spin state with a spin quantum number of 2.

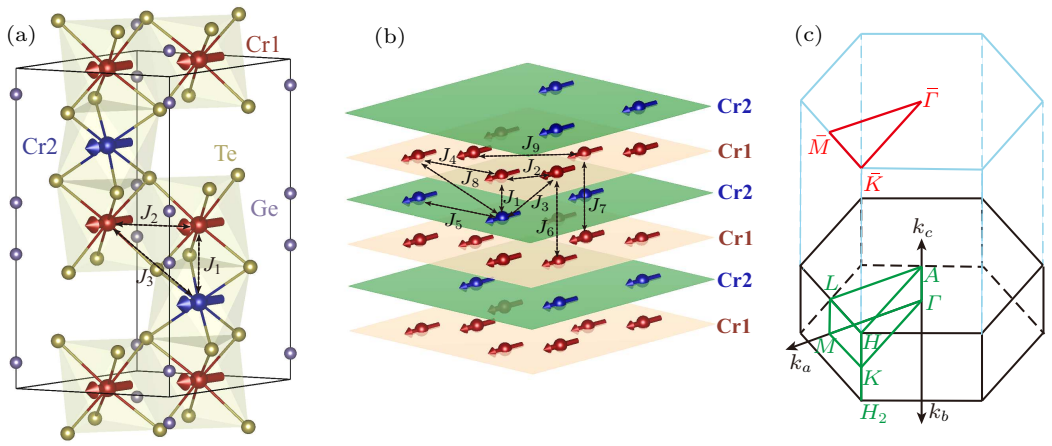


Fig. 1. (a) Side view of the self-intercalated structure of $Cr_3Ge_2Te_6$. $CrTe_6$ octahedra are shown by the dark yellow color. Double-headed arrows highlight the first three nearest-neighbor exchange paths. (b) Alternatingly stacked structure with only Cr atoms being shown. Cr1-honeycomb and Cr2-trigonal layers are indicated by light pink and green parallelograms, respectively. Double-headed arrows show the first nine nearest-neighbor exchange paths. (c) First Brillouin zone. Black lines and light blue lines represent the Brillouin zone of bulk and thin film, respectively. High-symmetry paths with labels for bulk and thin film are shown in green and red, respectively.

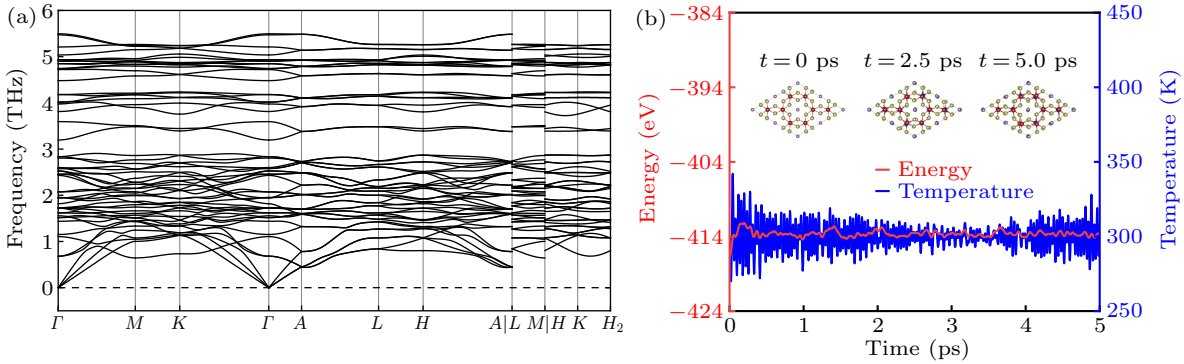


Fig. 2. Thermodynamical stability of $Cr_3Ge_2Te_6$. (a) Phonon spectrum along the high-symmetry paths. (b) Time-dependent evolutions of energy and temperature under the temperature of 300 K. Insets show the top views of the crystal structures of $Cr_3Ge_2Te_6$ at 0, 2.5 ps and 5.0 ps, respectively.

To confirm the thermodynamical stability of $Cr_3Ge_2Te_6$, we calculate its phonon spectrum with the finite displacement method[51] and perform *ab initio* molecular dynamic simulations at 300 K with the NVT canonical ensemble and a Nosé–Hoover thermostat.[52] Note that the magnetic ground state of the FM order (see the discussion below) is adopted in the phonon spectrum calculation. Figure 2(a) depicts the phonon dispersions along the high-symmetry paths shown in Fig. 1(c). One can see that there is no imaginary frequency in $Cr_3Ge_2Te_6$, suggesting that it is dynamically stable. Figure 2(b) shows the evolution of energy and temperature over time in *ab initio* molecular dynamic simulations. We see that the energy and temperature fluctuate around the equilibrium level. In addition, the crystal structure of $Cr_3Ge_2Te_6$ is not broken down in our simulation (see the insets in Fig. 2(b)). These all indicate that $Cr_3Ge_2Te_6$ is thermally stable at room temperature. Therefore, our calculations confirm that $Cr_3Ge_2Te_6$ is thermodynamically stable and can be synthesized in future experiments.

Here, we first investigate the magnetic properties of $Cr_3Ge_2Te_6$. To determine its magnetic ground state, we consider four typical magnetic orders of self-intercalated vdW structure. These orders are FM, FiM and two antiferromagnetic (denoted as AFM1 and AFM2, respectively) orders, which are depicted in Figs. 3(a)–3(d). Note that the AFM1 and AFM2 orders are two different types of antiferromagnetism with fully compensated magnetizations. As shown in Fig. 3(e), the calculated total energies of these four magnetic orders show that the FM order has the lowest total energy. Among them, the FiM and AFM1 orders have a significantly higher total energy than the FM order. Explicitly, their total energies are higher than that of the FM order by 152 meV/Cr and 198 meV/Cr, respectively. In short, our DFT-calculated results suggest that the FM order is the magnetic ground state of $Cr_3Ge_2Te_6$.

We employ a spin Hamiltonian that is composed of the first nine nearest-neighbor (NN) Heisenberg exchange interactions [see Fig. 1(b)] and magnetic anisotropy energy (MAE) to determine the T_C of $Cr_3Ge_2Te_6$. Our spin Hamiltonian has the following form:

$$H_{\text{spin}} = \sum_{i<j} J_{ij} \boldsymbol{S}_i \cdot \boldsymbol{S}_j + K \sum_i (S_i^z)^2, \tag{1}$$

where $\boldsymbol{S}_i$ and $\boldsymbol{S}_j$ are the spins at the magnetic sites i and j, respectively; the spin S_i^z is defined by the local z axis of

each ion i; J_{ij} is the Heisenberg exchange interactions, and K is the MAE constant. Antiferromagnetic (AFM) and FM Heisenberg interaction are characterized by a positive and negative J_{ij}, respectively. K is related to the energy difference $(E_z - E_x)$ between spin orientations of the z (E_z) and x (E_x) axes, with positive (negative) values of K representing in-plane (out-of-plane) magnetic anisotropy. As listed in Table 1, our calculations demonstrate that the values of Heisenberg exchange couplings are almost negative. Only three of them are relatively small positive, indicating that $Cr_3Ge_2Te_6$ is dominated by FM interactions. The first three NN Heisenberg exchange couplings are all FM, which is different from the strong magnetic frustration in $Mn_3Si_2Te_6$.[42] Within the Cr1-honeycomb layer, FM J_2 and J_9 are much stronger than AFM J_4. Thus, an FM order is formed in this layer. Although there is an AFM J_5 (6.44 meV) in the Cr2-trigonal layers, the FM J_3 (-41.60 meV) between Cr1-honeycomb layers and Cr2-trigonal layers is very strong. Consequently, an FM order is also formed in the Cr2-trigonal layer. The positive MAE (0.55 meV/Cr) indicates that $Cr_3Ge_2Te_6$ has an in-plane magnetic easy axis (i.e., the x axis). Lastly, our Monte Carlo simulations confirm that $Cr_3Ge_2Te_6$ has an in-plane FM magnetic ground state, with a T_C as high as 492 K. Hence, $Cr_3Ge_2Te_6$ is a room-temperature ferromagnet.

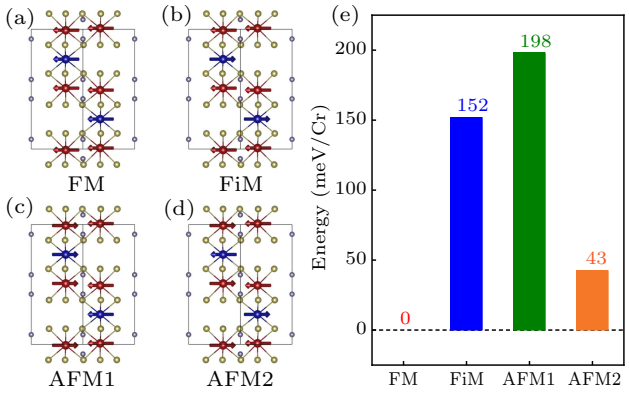


Fig. 3. Schematic of the considered four magnetic orders and DFT-calculated total energies. (a) FM, (b) FiM, (c) AFM1 and (d) AFM2 orders. (e) DFT-calculated total energies of the four magnetic orders. Total energy of the FM order is set as a reference.

Table 1. Magnetic parameters of $Cr_3Ge_2Te_6$ bulk and its 5L thin film. Heisenberg exchange interactions between two layers (i.e., Cr1-honeycomb and Cr2-trigonal layers) are classified in the column with heading 'Type'. The distances and values of nine NN exchange paths are in units of Å and meV, respectively. The MAE constant K and T_C are in units of meV/Cr and K, respectively. In 5L $Cr_3Ge_2Te_6$ thin film, distances of the first, third and eighth exchange paths (i.e., J_1, $J_3$and J_8) are respectively split into two slightly different values.

Exchange paths	Type	Bulk		5L	
		Distance	Value	Distance	Value
J_1	Cr1–Cr2	3.603	–0.76	3.729	–7.50
				3.731	–11.45
J_2	Cr1–Cr1	4.105	–9.22	4.073	–10.58
J_3	Cr1–Cr2	5.398	–41.60	5.471	–40.91
				5.516	–38.36
J_4	Cr1–Cr1	7.013	1.33	7.054	0.63
J_5	Cr2–Cr2	7.109	6.44	7.054	1.58
J_6	Cr1–Cr1	7.109	8.67	7.374	5.27
J_7	Cr1–Cr1	7.206	–3.11	7.46	–5.69
J_8	Cr1–Cr2	7.97	–0.40	7.979	0.71
				7.98	0.16
J_9	Cr1–Cr1	8.209	–9.30	8.145	–8.16
K		0.55		0.25	
T_C		492		409	
Magnetic ground state		FM		FM	

Now, we study the electronic properties of the FM $Cr_3Ge_2Te_6$. Our spin-resolved band structure, depicted in Fig. 4(a), shows that $Cr_3Ge_2Te_6$ is a metal. We find that the bands passing through the Fermi level are almost contributed by the majority states (i.e., spin up), while the conduction bands of minority states (i.e., spin down) around the high-symmetry points of K and H are slightly across the Fermi level. These features indicate that $Cr_3Ge_2Te_6$ is nearly half-metallic. To quantify this nearly half-metallicity in $Cr_3Ge_2Te_6$, we adopt the most commonly used definition of spin polarization (P) as follows:[53]

$$P = \frac{N_\uparrow - N_\downarrow}{N_\uparrow + N_\downarrow}, \tag{2}$$

where $N_\uparrow$ and $N_\downarrow$ are the total density of states (DOS) of majority and minority states at the Fermi level, respectively. For simplicity, the integral total DOS of 18 meV near the Fermi level [see the cyan area in Fig. 4(b)] from our DFT calculations is used to approximate the P. Based on Eq. (2), we obtain that $Cr_3Ge_2Te_6$ is nearly a half-metal with a high-spin polarization of up to 90.9%. In addition, atom-resolved DOS reveals that the bands around the Fermi level mainly come from Cr and Te atoms, implying the strong p–d hybridization between them [see Fig. 4(b)]. Figure 4(c) shows that the 3d orbitals of Cr^{2+} cations split into three distinct levels, consistent with the point group D_{3d} in $Cr_3Ge_2Te_6$. For a Cr^{2+} cation, its four 3d electrons are in a high-spin state and lead to 4 μ_B/Cr, align-

ing with our calculated magnetic moments. Considering the effect of strong SOC in Te atoms on electronic properties, we then examine the band structures of the FM $Cr_3Ge_2Te_6$ with SOC included in our DFT calculations. To obtain a deeper understanding of the effect of SOC, we set the magnetization of $Cr_3Ge_2Te_6$ along the x ($M \parallel x$) and z ($M \parallel z$) axes, respectively. As shown in Figs. 4(d) and 4(e), some crossing points and two-fold degenerate lines of bands are split. For instance, anti-crossing points along K–Γ (Γ–M) and gapped lines along A–L (Γ–A) occur in the case of $M \parallel x$ ($M \parallel z$). Thus, when combining the ferromagnetism with a strong SOC effect, some important properties, such as AHE, may be expected in $Cr_3Ge_2Te_6$.

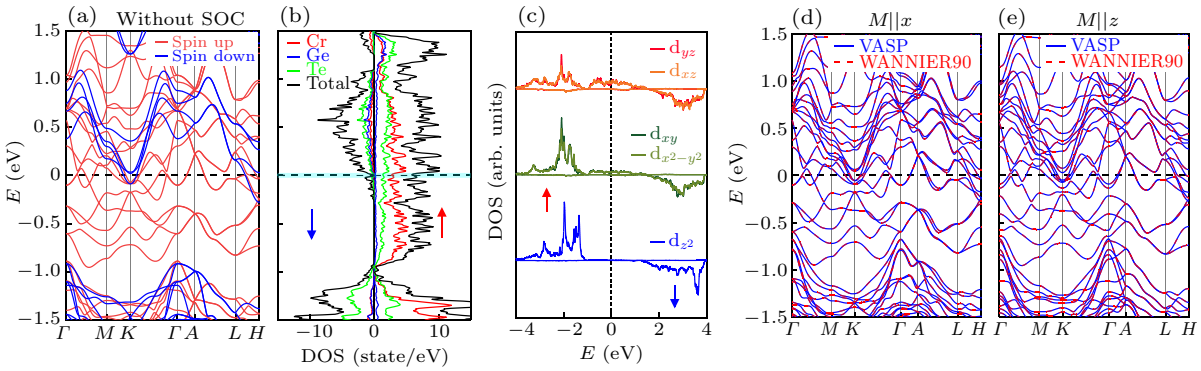


Fig. 4. Electronic properties of $Cr_3Ge_2Te_6$. (a) Spin-resolved band structure without SOC. (b) Atom-resolved DOS. Cyan energy interval around the Fermi level is used to integrate the total DOS. (c) 3d-orbital-resolved DOS. (d) Band structure in the case of $M \parallel x$ when SOC is considered. (e) The same as (d) except for the case of $M \parallel z$. In (d) and (e), DFT-calculated and Wannier-interpolated bands are represented by blue solid and red dash lines, respectively.

To investigate the underlying AHE in the FM $Cr_3Ge_2Te_6$, we construct an effective tight-binding model with the WANNIER90 package.[54] As shown in Figs. 4(d) and 4(e), the Wannier-interpolated bands fit well with those of DFT calculations. We then use the WannierTools package[55] to calculate the dependence of AHC on the position of the Fermi level of $Cr_3Ge_2Te_6$. As shown in Fig. 5(a), when the magnetization is along the easy axis (i.e., $M \parallel x$), the AHC component σ_{yz} of $Cr_3Ge_2Te_6$ is basically within 500 $\Omega^{-1}\cdot\mathrm{cm}^{-1}$. Given the weak MAE (0.55 meV/Cr) in $Cr_3Ge_2Te_6$, the magnetization can be easily regulated to the hard axis (i.e., $M \parallel z$) by applying an external magnetic field. Our calculations reveal that the AHC component σ_{xy} in the case of $M \parallel z$ is dramatically enlarged compared to the AHC component σ_{yz} in the case of $M \parallel x$. Specifically, σ_{xy} can reach a huge value of 1376 $\Omega^{-1}\cdot\mathrm{cm}^{-1}$ when the Fermi level is located at 0.5 eV [Fig. 5(b)].

For practical applications, the AHC near the Fermi level is crucial. We thus further study the AHC of $Cr_3Ge_2Te_6$ with the Fermi level ranging from −0.1 eV to 0.1 eV [see cyan areas in Figs. 5(a) and 5(b)]. Figure 5(c) shows the detailed dependence of AHCs on the Fermi level in this range. In the case of $M \parallel x$, $Cr_3Ge_2Te_6$ has an AHC of 138 $\Omega^{-1}\cdot\mathrm{cm}^{-1}$ when the Fermi level is located at zero. We also find that the AHC almost monotonically increases to 318 $\Omega^{-1}\cdot\mathrm{cm}^{-1}$ when the Fermi level is gradually tuned to 70 meV. In experiments, this could be realized through doping electrons into $Cr_3Ge_2Te_6$, e.g., the substitution of arsenic atoms for germanium atoms. In the case of $M \parallel z$, the AHC at the Fermi level is up to 305 $\Omega^{-1}\cdot\mathrm{cm}^{-1}$. Surprisingly, the AHC can reach as large as 648 $\Omega^{-1}\cdot\mathrm{cm}^{-1}$ when the Fermi level is located at −90 meV. Similarly, doping gallium atoms in the Ge sites of $Cr_3Ge_2Te_6$ should be appealing to realize such large AHE in experiments. The large AHC of the FM $Cr_3Ge_2Te_6$, which can be tuned by regulating its magnetization or doping, makes it very suitable for designing advanced spintronic devices.

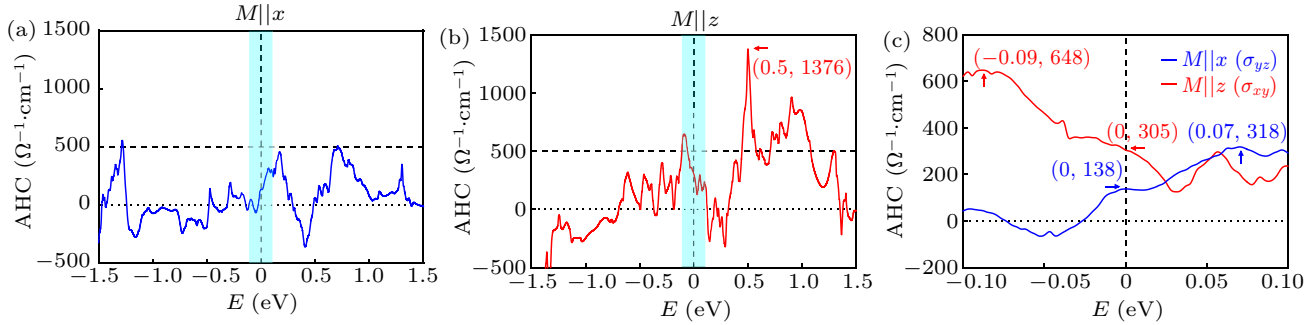


Fig. 5. Dependence of AHC on the position of the Fermi level. (a) AHC component σ_{yz} in the case of $M \parallel x$. (b) AHC component σ_{xy} in the case of $M \parallel z$. In (a) and (b), the Fermi level range from −0.1 eV to 0.1 eV is highlighted by the cyan areas. (c) Zoomed-in AHC σ_{yz} and σ_{xy}. In (b) and (c), the first and second numbers inside the brackets are the values of the Fermi level and AHC, respectively.

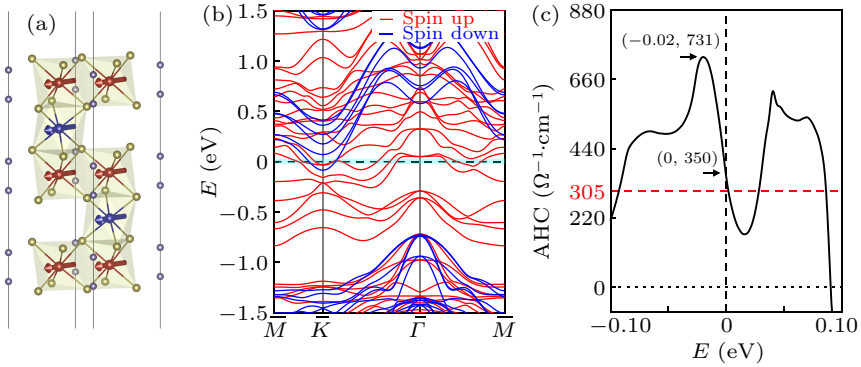


Fig. 6. Crystal and electronic properties of 5L $Cr_3Ge_2Te_6$ thin film. (a) Side view of the crystal structure. (b) Spin-resolved band structure without SOC. Energy interval highlighted by cyan around the Fermi level is used to calculate spin polarization, P. (c) AHC components, σ_{xy}, when the 5L $Cr_3Ge_2Te_6$ thin film has an out-of-plane magnetization. The AHC components σ_{xy} of $Cr_3Ge_2Te_6$ bulk in the case of $M \parallel z$ with its Fermi level being located at zero is highlighted by a red dash line. The first and second numbers in the brackets are the values of the Fermi level and AHC, respectively.

Over recent decades, the development of highly sensitive and miniaturized magnetic devices has become more and more important. We thereby investigate the magnetic and electronic properties of $Cr_3Ge_2Te_6$ thin film with 5L thickness [Fig. 6(a)]. To determine the magnetic ground state and T_C of 5L $Cr_3Ge_2Te_6$ thin film, we calculate its magnetic parameters based on Hamiltonian (1). As listed in Table 1, the first nine NN Heisenberg exchange interactions of 5L $Cr_3Ge_2Te_6$ thin film are dominated by FM couplings whose values are much larger than those of AFM couplings. Due to these much stronger FM couplings, our Monte Carlo simulations reveal that 5L $Cr_3Ge_2Te_6$ thin film has an FM magnetic ground state with a T_C of 409 K. Compared with the $Cr_3Ge_2Te_6$ bulk, 5L $Cr_3Ge_2Te_6$ thin film has a smaller MAE of 0.25 meV/Cr. Hence, it should be easier to regulate the magnetic moment towards the hard axis (i.e., $M \parallel z$) by applying an external magnetic field to the 5L $Cr_3Ge_2Te_6$ thin film.

Figure 6(b) depicts the spin-resolved FM band structure of the 5L $Cr_3Ge_2Te_6$ thin film. There is only one band of minority states (i.e., spin down) around the high-symmetry point of $\bar{K}$ across the Fermi level, indicating that the 5L $Cr_3Ge_2Te_6$ thin film could have a higher spin polarization. Our calculation of the spin polarization from the integral total DOS of 18 meV near the Fermi level [see the cyan energy interval in Fig. 6(b)] indicates that the spin polarization of the 5L $Cr_3Ge_2Te_6$ thin film is as large as 99.8%. When the 5L $Cr_3Ge_2Te_6$ thin film has an out-of-plane magnetization, it has a greater AHC of 350 $\Omega^{-1} \cdot \mathrm{cm}^{-1}$, compared with that (305 $\Omega^{-1} \cdot \mathrm{cm}^{-1}$) of $Cr_3Ge_2Te_6$ bulk [see Fig. 6(c)]. Surprisingly, the AHC of the 5L $Cr_3Ge_2Te_6$ thin film can reach up to 731 $\Omega^{-1} \cdot \mathrm{cm}^{-1}$ when its Fermi level is located at -20 meV. This means it is easier to achieve larger AHE by doping holes into the 5L $Cr_3Ge_2Te_6$ thin film in experiments. Therefore, the nearly half-metallic ferromagnetism with a high T_C above room temperature and larger AHC shows that the 5L $Cr_3Ge_2Te_6$ thin film has great promise for designing advanced nano-scale electronic devices.

4. Conclusion

In summary, using the first-principles study and Monte Carlo simulations, we systematically investigate the magnetic and electronic properties of the self-intercalated vdW magnet, $Cr_3Ge_2Te_6$. Our calculations reveal that $Cr_3Ge_2Te_6$ is thermodynamically stable and that it is a room-temperature in-plane ferromagnet with a high T_C of 492 K. By scrutinizing the electronic structure of the FM $Cr_3Ge_2Te_6$, we find that its spin polarization reaches 90.9%, indicating its near half-metallicity in $Cr_3Ge_2Te_6$. Due to its ferromagnetism and the strong SOC effect, $Cr_3Ge_2Te_6$ exhibits AHCs of 138 $\Omega^{-1} \cdot \mathrm{cm}^{-1}$ and 305 $\Omega^{-1} \cdot \mathrm{cm}^{-1}$ when its magnetization is along the x and z axes, respectively. Furthermore, these AHCs can be dramatically increased by doping holes or electrons in experiments. Lastly, the 5L $Cr_3Ge_2Te_6$ thin film also possesses in-plane ferromagnetism with a high T_C above room temperature. More interestingly, the 5L $Cr_3Ge_2Te_6$ thin film shows better performance with a higher spin polarization and larger AHC, compared with $Cr_3Ge_2Te_6$ bulk. Our work demonstrates a novel self-intercalated $Cr_3Ge_2Te_6$, which has room-temperature ferromagnetism, high-spin polarization, large AHC, and may provide great opportunities for designing advanced nano-scale spintronic devices.

Acknowledgements

Project supported by the National Key R&D Program of China (Grant No. 2022YFA1403301), the National Natural Science Foundation of China (Grant Nos. 12474247 and 92165204) and the Guangdong Provincial Key Laboratory of Magnetoelectric Physics and Devices (Grant No. 2022B1212010008). Yusheng Hou acknowledges the support from the Fundamental Research Funds for the Central Universities, Sun Yat-Sen University (Grant No. 24qnpy108).

References

[1] Novoselov K S, Geim A K, Morozov S V, Jiang D E, Zhang Y, Dubonos S V, Grigorieva I V and Firsov A A 2004 *Science* **306** 666
[2] Duong D L, Yun S J and Lee Y H 2017 *ACS Nano* **11** 11803
[3] Lin Z, Peng Y, Wu B, Wang C, Luo Z and Yang J 2022 *Chin. Phys. B* **31** 087506
[4] Zhang W, Wong P K J, Zhu R and Wee A T S 2019 *InfoMat* **1** 479
[5] Zhang X, Wang J, Zhu W, Zhang J, Li W, Zhang J and Wang K 2024 *Chin. Phys. Lett.* **41** 067503
[6] Zhu W, Xie S, Lin H, Zhang G, Wu H, Hu T, Wang Z, Zhang X, Xu J, Wang Y, Zheng Y, Yan F, Zhang J, Zhao L, Patané A, Zhang J, Chang H and Wang K 2022 *Chin. Phys. Lett.* **39** 128501
[7] Burch K S, Mandrus D and Park J G 2018 *Nature* **563** 47
[8] Huang B, Clark G, Navarro-Moratalla E, Klein D R, Cheng R, Seyler K L, Zhong D, Schmidgall E, McGuire M A, Cobden D H, Yao W, Xiao D, Jarillo-Herrero P and Xu X 2017 *Nature* **546** 270
[9] Gong C, Li L, Li Z, Ji H, Stern A, Xia Y, Cao T, Bao W, Wang C, Wang Y, Qiu Z Q, Cava R J, Louie S G, Xia J and Zhang X 2017 *Nature* **546** 265
[10] Wang N, Tang H, Shi M, Zhang H, Zhuo W, Liu D, Meng F, Ma L, Ying J, Zou L, Sun Z and Chen X 2019 *J. Am. Chem. Soc.* **141** 17166
[11] Wang Z, Zheng H, Chen A, Ma L, Hong S J, Rodriguez E E, Woehl T J, Shi S F, Parker T and Ren S 2024 *ACS Nano* **18** 23058
[12] Yang R, Mei L, Lin Z, Fan Y, Lim J, Guo J, Liu Y, Shin H S, Voiry D, Lu Q, Li J and Zeng Z 2024 *Nature Reviews Chemistry* **8** 410
[13] Zhao X, Song P, Wang C, Riis-Jensen A C, Fu W, Deng Y, Wan D, Kang L, Ning S, Dan J, Venkatesan T, Liu Z, Zhou W, Thygesen K S, Luo X, Pennycook S J and Loh K P 2020 *Nature* **581** 171
[14] Coughlin A L, Xie D, Zhan X, Yao Y, Deng L, Hewa-Walpitage H, Bontke T, Chu C W, Li Y, Wang J, Fertig H A and Zhang S 2021 *Nano Lett.* **21** 9517
[15] Liu Y and Petrovic C 2018 *Phys. Rev. B* **98** 195122
[16] Liu Y, Abeykoon M, Stavitski E, Attenkofer K and Petrovic C 2019 *Phys. Rev. B* **100** 245114
[17] Tang B, Wang X, Han M, Xu X, Zhang Z, Zhu C, Cao X, Yang Y, Fu Q, Yang J, Li X, Gao W, Zhou J, Lin J and Liu Z 2022 *Nat. Electron.* **5** 224
[18] Miao W T, Zhen W L, Lu Z, Wang H N, Wang J, Niu Q and Tian M L 2024 *Chin. Phys. Lett.* **41** 067501
[19] Zhao D, Zhang L, Malik I A, Liao M, Cui W, Cai X, Zheng C, Li L, Hu X, Zhang D, Zhang J, Chen X, Jiang W and Xue Q 2018 *Nano Research* **11** 3116
[20] Saha R, Meyerheim H L, Göbel B, Hazra B K, Deniz H, Mohseni K, Antonov V, Ernst A, Knyazev D, Bedoya-Pinto A, Mertig I and Parkin S S P 2022 *Nat. Commun.* **13** 3965
[21] Li B, Deng X, Shu W, Cheng X, Qian Q, Wan Z, Zhao B, Shen X, Wu R, Shi S, Zhang H, Zhang Z, Yang X, Zhang J, Zhong M, Xia Q, Li J, Liu Y, Liao L, Ye Y, Dai L, Peng Y, Li B and Duan X 2022 *Materials Today* **57** 66
[22] Zhang C, Liu C, Zhang J, Yuan Y, Wen Y, Li Y, Zheng D, Zhang Q, Hou Z, Yin G, Liu K, Peng Y and Zhang X X 2023 *Adv. Mater.* **35** 2205967
[23] Seo J, De C, Ha H, Lee J E, Park S, Park J, Skourski Y, Choi E S, Kim B, Cho G Y, Yeom H W, Cheong S W, Kim J H, Yang B J, Kim K and Kim J S 2021 *Nature* **599** 576
[24] Ni Y, Zhao H, Zhang Y, Hu B, Kimchi I and Cao G 2021 *Phys. Rev. B* **103** L161105
[25] Ye F, Matsuda M, Morgan Z, Sherline T, Ni Y, Zhao H and Cao G 2022 *Phys. Rev. B* **106** L180402
[26] Zhang Y, Ni Y, Zhao H, Hakani S, Ye F, DeLong L, Kimchi I and Cao G 2022 *Nature* **611** 467
[27] Wang J, Wang S, He X, Zhou Y, An C, Zhang M, Zhou Y, Han Y, Chen X, Zhou J and Yang Z 2022 *Phys. Rev. B* **106** 045106
[28] Zhang Y, Lin L F, Moreo A and Dagotto E 2023 *Phys. Rev. B* **107** 054430
[29] Olmos R, Chang P H, Mishra P, Zope R R, Baruah T, Liu Y, Petrovic C and Singamaneni S R 2023 *The Journal of Physical Chemistry C* **127** 10324
[30] Gu Y, Smith K A, Saha A, De C, Won C J, Zhang Y, Lin L F, Cheong S W, Haule K, Ozerov M, Birol T, Homes C, Dagotto E and Musfeldt J L 2024 *Nat. Commun.* **15** 8104
[31] Tan C, Deng M, Yang Y, An L, Ge W, Albarakati S, Panahandeh-Fard M, Partridge J, Culcer D, Lei B, Wu T, Zhu X, Tian M, Chen X, Wang R Q and Wang L 2024 *Nano Lett.* **24** 4158
[32] Susilo R A, Kwon C I, Lee Y, Salke N P, De C, Seo J, Kang B, Hemley R J, Dalladay-Simpson P, Wang Z, Kim D Y, Kim K, Cheong S W, Yeom H W, Kim K H and Kim J S 2024 *Nat. Commun.* **15** 3998
[33] Huang C, Huo M, Huang X, Liu H, Li L, Zhang Z, Chen Z, Han Y, Chen L, Liang F, Dong H, Shen B, Sun H and Wang M 2024 *Phys. Rev. B* **109** 205145
[34] Zhang Y, Ni Y, Schlottmann P, Nandkishore R, DeLong L E and Cao G 2024 *Nat. Commun.* **15** 3579
[35] Li D, Wang M, Li D and Zhou J 2024 *Phys. Rev. B* **109** 155153
[36] Liu Y and Petrovic C 2018 *Phys. Rev. B* **98** 064423
[37] Liu Y, Hu Z, Abeykoon M, Stavitski E, Attenkofer K, Bauer E D and Petrovic C 2021 *Phys. Rev. B* **103** 245122
[38] Li Q, Cheng Y, Zhao D, Huang Y, Wan X and Zhou J 2023 *New J. Phys.* **25** 103020
[39] Ran C, Mi X, Shen J, Wang H, Yang K, Liu Y, Wang G, Wang G, Shi Y, Wang A, Chai Y, Yang X, He M, Tong X and Zhou X 2023 *Phys. Rev. B* **108** 125103
[40] Wu Q, Yin Q, Zhang S, Hu T, Wu D, Yue L, Li B, Xu S, Li R, Liu Q, Lei H, Dong T and Wang N 2024 *Advanced Optical Materials* **12** 2301863
[41] Yin Y, Wan X, Tu X and Wang D 2024 *Phys. Rev. B* **110** 104410
[42] May A F, Liu Y, Calder S, Parker D S, Pandey T, Cakmak E, Cao H, Yan J and McGuire M A 2017 *Phys. Rev. B* **95** 174440
[43] Qiao L, Barone P, Yang B, King P D C, Ren W and Picozzi S 2024 *Physical Chemistry Chemical Physics* **26** 8604
[44] Kresse G and Furthmüller J 1996 *Phys. Rev. B* **54** 11169
[45] Perdew J P, Burke K and Ernzerhof M 1996 *Phys. Rev. Lett.* **77** 3865
[46] Blöchl P E 1994 *Phys. Rev. B* **50** 17953
[47] Kresse G and Joubert D 1999 *Phys. Rev. B* **59** 1758
[48] Liechtenstein A, Anisimov V I and Zaanen J 1995 *Phys. Rev. B* **52** R5467
[49] Moulkhalwa H, Zaoui Y, Obodo K O, Belkadi A, Beldi L and Bouhafs B 2019 *Journal of Superconductivity and Novel Magnetism* **32** 635
[50] Hao Z, Li H, Zhang S, Li X, Lin G, Luo X, Sun Y, Liu Z and Wang Y 2018 *Science Bulletin* **63** 825
[51] Kresse G, Furthmüller J and Hafner J 1995 *Europhys. Lett.* **32** 729
[52] Nosé S 1984 *The Journal of Chemical Physics* **81** 511
[53] Mazin I I 1999 *Phys. Rev. Lett.* **83** 1427
[54] Mostofi A A, Yates J R, Lee Y S, Souza I, Vanderbilt D and Marzari N 2008 *Computer Physics Communications* **178** 685
[55] Wu Q, Zhang S, Song H F, Troyer M and Soluyanov A A 2018 *Computer Physics Communications* **224** 405